Journal of Marine Science and Technology

Volume 22 | Issue 2 Article 13

SHAPE OPTIMIZATION OF MULTI-CHAMBER PLENUMS WITH MULTI-LAYER SOUND ABSORERS USING AN ARTIFICIAL IMMUNE METHOD

Min-Chie Chiu
Department of Mechanical and Automation Engineering, Chung Chou University of Science and Technology, Changhua County, Taiwan, R.O.C, minchie.chiu@msa.hinet.net

Recommended Citation
Chiu, Min-Chie (2014) "SHAPE OPTIMIZATION OF MULTI-CHAMBER PLENUMS WITH MULTI-LAYER SOUND ABSORERS USING AN ARTIFICIAL IMMUNE METHOD," *Journal of Marine Science and Technology*: Vol. 22: Iss. 2, Article 13.
DOI: 10.6119/JMST-013-0503-2
Available at: https://jmstt.ntou.edu.tw/journal/vol22/iss2/13

SHAPE OPTIMIZATION OF MULTI-CHAMBER PLENUMS WITH MULTI-LAYER SOUND ABSORERS USING AN ARTIFICIAL IMMUNE METHOD

Acknowledgements

The author acknowledges the financial support of the National Science Council (NSC100-2622-E-235-001-CC3, Taiwan, ROC).

Journal of Marine Science and Technology, Vol. 22, No. 2, pp. 218-230 (2014)
DOI: 10.6119/JMST-013-0503-2

SHAPE OPTIMIZATION OF MULTI-CHAMBER PLENUMS WITH MULTI-LAYER SOUND ABSORBERS USING AN ARTIFICIAL IMMUNE METHOD

Min-Chie Chiu

Key words: multi-chamber plenum, multi-layer sound absorber, artificial immune method, optimization, space-constrained.

ABSTRACT

Because of the space constraints problem in practical engineering work, there is a growing need to optimize the acoustical performance of a sound-proofing device within a fixed space. The optimal mechanism used in adjusting either the plenum's chamber or an internal sound absorber has been ignored. In order to maximize the acoustical performance of a plenum, a case study of depressing a diesel engine noise by using three kinds of optimally shaped multi-chamber acoustical plenums lined with three kinds of multi-layer sound absorbers is introduced. On the basis of constrained weight and space in the plenum, a low cost optimal acoustical mechanism was assessed using an artificial immune method (*AIM*).

Consequently, this paper provides a quick, economical, and effective method for reducing noise levels by optimally designing shaped multi-chamber acoustical plenums lined with multi-layer sound absorbers using an artificial immune method.

I. INTRODUCTION

Research on the acoustical plenum has been widely discussed. Ko [17] started the study of sound transmission loss (*STL*) for a rectangular tube that had both the upper and the lower sides lined with perforated sound absorbing material. Blair and Coates [3] assessed the *STL* of a venting system based on the linear acoustic theory. Later, a sound attenuation loss of a rectangular tube lined with sound absorbing material on two or four sides of the tube was proposed. [22]. At the same time, the influence of noise reduction with respect to different flow rates was also analyzed [10]. Afterward, a new technology to reduce the *STL* of a one-chamber plenum by lining the instrument with sound absorbing material was advanced [2]. Also, the acoustical performance of a side inlet/outlet plenum using a plane wave theory was suggested [25]. Moreover, the acoustical performance of a rectangular plenum using both theoretical and experimental data was analyzed [20]. Furthermore, the influence of a plenum's acoustical performance with respect to the perforated hole's distance using a finite element method was assessed [21].

There is a growing need to optimize the acoustical performance within a fixed space. However, the research work of optimally shaped multi-chamber acoustical plenum within a space-constrained situation has been overlooked. In order to efficiently maximize the acoustical performance of a multi-chamber plenum, a numerical assessment in finding three kinds of optimally shaped multi-chamber acoustical plenum (one-chamber, two-chamber, and three-chamber) lined with three kinds of multi-layer sound absorbers (one-layer, two-layer, and three-layer) utilizing an artificial immune method (*AIM*) will be presented. Here, to facilitate the numerical assessment, not only the theoretical formula [2] in predicting an acoustical plenum's *STL* but also the formula in predicting the sound absorbing coefficient of a multi-layer sound absorber [6] will be linked and adopted in the mathematical model. Moreover, to maintain the lowest manufacturing cost in the plenum, the total thickness of the perforated plates and the sound absorbing material inside the sound absorber will be fixed in advance.

II. MATHEMATICAL MODELS

A multi-chamber acoustical plenum internally lined with multi-layer sound absorbers shown in Fig. 1 is adopted to reduce the noise emitted from a diesel engine. The mathematical model for the multi-chamber acoustical plenum is described below.

1. The One-chamber Acoustical Plenum

As indicated in Fig. 2, for a multi-chamber plenum inter-

Paper submitted 11/15/11; revised 02/05/13; accepted 05/03/13. *Author for correspondence: Min-Chie Chiu (e-mail: minchie.chiu@msa.hinet.net).*
Department of Mechanical and Automation Engineering, Chung Chou University of Science and Technology, Yuanlin, Changhua County, Taiwan, R.O.C.

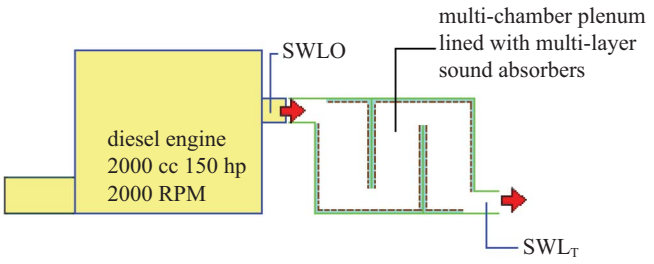

Fig. 1. The noise control of a diesel engine using a multi-chamber plenum lined with a multi-layer sound absorber.

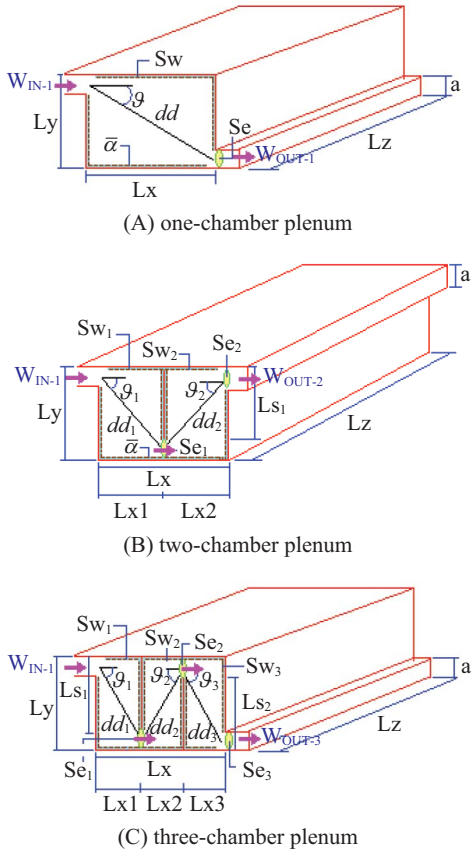

Fig. 2. The outline dimensions for three kinds of multi-chamber plenums lined with multi-layer sound absorbers.

nally lined with sound absorbing material, the reverberant sound power (W_{rf}) at the outlet of the *i*-th chamber plenum is [2]

$$W_{rf-i} = W_{IN-i} S_{e-i} / R_i \tag{1a}$$

where

$$R_i = S_{w-i}\bar{\alpha}_i / (1-\bar{\alpha}_i) \tag{1b}$$

For the *i*-th chamber of the plenum, the direct sound power (W_{df-i}) at the outlet is

$$W_{df-i} = W_{IN-i} S_{e-i} \cos\vartheta_i / 2\pi dd_i^2 \tag{2}$$

Combining Eq. (1a) with Eq. (2), the total sound power (W_{OUT-i}) at the outlet of the *i*-th chamber plenum is

$$\begin{aligned} W_{OUT-i} &= W_{rf-i} + W_{df-i} \\ &= W_{IN-i}(S_{e-i}/R_i + S_{e-i}\cos\vartheta_i / 2\pi dd_i^2) \end{aligned} \tag{3}$$

For a n-chamber plenum, the total sound power (W_{OUT-i}) at the outlet of the *n*-th chamber plenum is

$$\begin{aligned} W_{OUT-n} &= W_{rf-n} + W_{df-n} \\ &= W_{IN-n}(S_{e-n}/R_n + S_{e-n}\cos\vartheta_n / 2\pi dd_n^2) \end{aligned} \tag{4}$$

where $W_{IN-n} = W_{OUT-(n-1)}$

Therefore, the substitution of W_{OUT-n} can be expressed as

$$\begin{aligned} W_{OUT-n} &= W_{IN-n}(S_{e-n}/R_n + S_{e-n}\cos\vartheta_n / 2\pi dd_n^2) \\ &= W_{IN-1}\sum_{i=1}^{n}\left(\frac{S_{e-i}}{R_i} + \frac{S_{e-i}\cos\vartheta_i}{2\pi dd_i^2}\right) \end{aligned} \tag{5}$$

According the definition of sound transmission, the STL for an n-chamber plenum is

$$\begin{aligned} STL_n(\bar{X}) &= -10\log_{10}\frac{W_{OUT-n}}{W_{IN-1}} \\ &= 10\log_{10}\sum_{i=1}^{n}\left(\frac{1}{S_{e-i}\left(\frac{1-\bar{\alpha}_i}{S_{w-i}\bar{\alpha}_i} + \frac{\cos\vartheta_i}{2\pi dd_i^2}\right)}\right) \end{aligned} \tag{6a}$$

$$\bar{X} = (\bar{\alpha}(f); S_{e-1},...S_{e-n}; S_{w-1},...,S_{w-n}; dd_1,...,dd_n) \tag{6b}$$

where S_e is the outlet area, S_w is the total inner area of the plenum, $\bar{\alpha}$ is the average sound absorption coefficient within a plenum, *dd* is the distance between the inlet and the outlet of the plenum, and ϑ is the angle between the diagonal line (from plenum inlet to plenum outlet) and the horizontal line.

2. The Sound Absorption Coefficients for Multi-layer Sound Absorber

Four kinds of multi-layer sound absorbers (one-layer, two-layer, and three-layer) inside the inner wall of the plenum are shown in Fig. 3. The derivation of sound absorption coefficients with respect to the three kinds of multi-layer sound absorbers are described below.

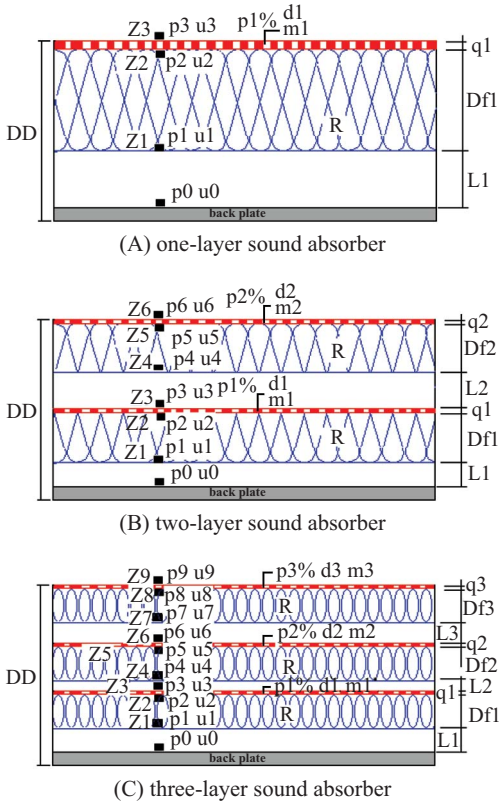

Fig. 3. The outline dimensions for three kinds of multi-layer sound absorbers (A: one-layer; B: two-layer; C: three-layer).

1) A One-layer Sound Absorber

As indicated in Fig. 3(A), the acoustic impedance on the perforated front plate is obtained from the bottom wall where the value of the impedance is infinity. There are four points representing the absorbing impedance within the absorber. The absorber is composed of a structure of "rigid-backing plate + L_i thickness of air + D_{fi} thickness of the acoustic fiber + q_1 thickness of the perforated front plate." As derived in a previous study [6], for a wave propagating normally in a quiescent medium symbolized by "*m*," the general matrix form between point *i* and point *i*+1 is expressed as

$$\begin{pmatrix} p_{i+1} \\ u_{i+1} \end{pmatrix} = \begin{bmatrix} \cos(k_m L) & jZ_m \sin(k_m L) \\ j\dfrac{1}{Z_m}\sin(k_m L) & \cos(k_m L) \end{bmatrix} \begin{pmatrix} p_i \\ u_i \end{pmatrix} \tag{7}$$

Therefore, the relationship of the acoustic pressure *p* and the acoustic particle velocity *u* between point 0 and point 1 is expressed as the transfer matrix and shown below.

$$\begin{pmatrix} p_1 \\ u_1 \end{pmatrix} = \begin{bmatrix} \cos(\omega L_1/c_o) & j\rho_o c_o \sin(\omega L_1/c_o) \\ j\dfrac{\sin(\omega L_1/c_o)}{\rho_o c_o} & \cos(\omega L_1/c_o) \end{bmatrix} \begin{pmatrix} p_o \\ u_o \end{pmatrix} \tag{8}$$

Developing Eq. (8) yields

$$Z_1 = -j\rho_o c_o \cot\left(\frac{\omega L_1}{c_o}\right) \tag{9}$$

The relationship of the acoustic pressure *p* and the acoustic particle velocity *u* with respect to points 1 and 2 is expressed in the transfer matrices below.

$$\begin{pmatrix} p_2 \\ u_2 \end{pmatrix} = \begin{bmatrix} \cos\left(k_{fiber-1}D_{f1}\right) & jZ_{fiber-1}\sin\left(k_{fiber-1}D_{f1}\right) \\ j\dfrac{1}{Z_{fiber-1}}\sin\left(k_{fiber-1}D_{f1}\right) & \cos\left(k_{fiber-1}D_{f1}\right) \end{bmatrix} \begin{pmatrix} p_1 \\ u_1 \end{pmatrix} \tag{10}$$

By developing Eq. (10), an alternative form of Eq. (10) yields

$$Z_2\left(=\frac{p_2}{u_2}\right) = Z_{fiber-1}\frac{Z_1\cosh[k_{fiber-1}D_{f1}]+Z_{fiber-1}\sinh[k_{fiber-1}D_{f1}]}{Z_1\sinh[k_{fiber-1}D_{f1}]+Z_{fiber-1}\cosh[k_{fiber-1}D_{f1}]} \tag{11}$$

By adopting the formula of the specific normal impedance and wave number [9], Eq. (11) is written as

$$Z_2 = \left(R_{fiber-1}+jX_{fiber-1}\right)\begin{bmatrix} \sinh(k_{21}D_{f1})\cos(k_{11}D_{f1}) - \\ j\sin(k_{11}D_{f1})\cosh(k_{21}D_{f1}) \\ \hline \cos(k_{11}D_{f1})\cosh(k_{21}D_{f1}) - \\ j\sinh(k_{21}D_{f1})\sin(k_{11}D_{f1}) \end{bmatrix} \tag{12}$$

For sound flowing into the perforated plate, it is assumed that the incident sound passes through the holes of the perforated plate and is immediately transmitted to the porous material behind the perforated plate [19, 24]. The continuity of the particle velocity is then applied and expressed as

$$u_2 = u_3 \tag{13}$$

Acoustic impedance yields

$$p_3 = Z_{p_1}u_2 + p_2 \tag{14}$$

Combining Eqs. (13)~(14), the transfer matrix between point 2 and point 3 yields

$$\begin{pmatrix} p_3 \\ u_3 \end{pmatrix} = \begin{bmatrix} 1 & Z_{p1} \\ 0 & 1 \end{bmatrix} \begin{pmatrix} p_2 \\ u_2 \end{pmatrix} \tag{15}$$

Developing Eq. (15) and substituting Eq. (7), the specific normal impedance at point 3 is

$$Z_3 = Z_2 + Z_{p1} \tag{16}$$

Adopting the specific normal impedance and wave number of the perforated plate [1] yields

$$Z_{p1} = \frac{\rho_o}{\varepsilon_1}\sqrt{8\nu\omega}\left(1+\frac{q_1}{2d_1}\right)+ j\frac{\omega\rho_o}{\varepsilon_1}\left[\sqrt{\frac{8\nu}{\omega}}\left(1+\frac{q_1}{2d_1}\right)+q_1+\delta_1\right] \tag{17a}$$

$$\delta_1 = 0.85(2d_1)\left(1-1.47\sqrt{\varepsilon_1}+0.47\sqrt{\varepsilon_1^3}\right) \tag{17b}$$

For normal incidence, the sound absorption coefficient [14, 19, 24] is

$$\alpha_1(f,\varepsilon_1,d_1,R_1,q_1,D_{f1},L_1,DD)$$

$$=1-\left|\frac{Z_3-\rho_o c_o}{Z_3+\rho_o c_o}\right|^2 = \alpha_1(f,p_1\%,d_1,R_1,q_1,D_{f1},L_1,DD) \tag{18}$$

2) A Two-layer Sound Absorber

Similarly, for a two-layer sound absorber shown in Fig. 3(B), the acoustical impedance at point 5 is

$$Z_5\left(=\frac{p_5}{u_5}\right) = Z_{fiber-2}\frac{Z_4\cosh[k_{fiber-2}D_{f2}]+Z_{fiber-2}\sinh[k_{fiber-2}D_{f2}]}{Z_4\sinh[k_{fiber-2}D_{f2}]+Z_{fiber-2}\cosh[k_{fiber-2}D_{f2}]}$$

$$Z_2 = \left(R_{fiber-2}+jX_{fiber-2}\right)\begin{bmatrix}\sinh(k_{22}D_{f2})\cos(k_{12}D_{f2})-\\ j\sin(k_{12}D_{f2})\cosh(k_{22}D_{f2})\\ \cos(k_{12}D_{f2})\cosh(k_{22}D_{f2})-\\ j\sinh(k_{22}D_{f2})\sin(k_{12}D_{f2})\end{bmatrix} \tag{19}$$

For sound flowing into the 2nd perforated plate, the transfer matrix between point 5 and point 6 yields

$$\begin{pmatrix}p_6\\u_6\end{pmatrix}=\begin{bmatrix}1 & Z_{p2}\\0 & 1\end{bmatrix}\begin{pmatrix}p_5\\u_5\end{pmatrix} \tag{20}$$

The specific normal impedance at point 6 is

$$Z_6 = Z_5 + Z_{p2} \tag{21}$$

For normal incidence, the sound absorption coefficient [14, 19, 24] is

$$\alpha_2(f,\varepsilon_1,\varepsilon_2,d_1,d_2,R_1,R_2,q_1,q_2,D_{f1},D_{f2},L_1,L_2,DD)$$

$$=1-\left|\frac{Z_6-\rho_o c_o}{Z_6+\rho_o c_o}\right|^2$$

$$=\alpha_2(f,p_1\%,p_2\%,d_1,d_2,R_1,R_2,q_1,q_2,D_{f1},D_{f2},L_1,L_2,DD) \tag{22}$$

3) A Three-layer Sound Absorber

Likewise, for a three-layer sound absorber shown in Fig. 3(C), the acoustical impedance at point 8 is

$$Z_8 = Z_{fiber-3}\frac{Z_7\cosh[k_{fiber-3}D_{f3}]+Z_{fiber-3}\sinh[k_{fiber-3}D_{f3}]}{Z_7\sinh[k_{fiber-3}D_{f3}]+Z_{fiber-3}\cosh[k_{fiber-3}D_{f3}]}$$

$$Z_2 = \left(R_{fiber-3}+jX_{fiber-3}\right)\begin{bmatrix}\sinh(k_{23}D_{f3})\cos(k_{13}D_{f3})-\\ j\sin(k_{13}D_{f3})\cosh(k_{23}D_{f3})\\ \cos(k_{13}D_{f3})\cosh(k_{23}D_{f3})-\\ j\sinh(k_{23}D_{f3})\sin(k_{13}D_{f3})\end{bmatrix} \tag{23}$$

The specific normal impedance at point 9 is

$$Z_9 = Z_8 + Z_{p3} \tag{24}$$

For normal incidence, the sound absorption coefficient [14, 19, 24] is

$$\alpha_3(f,\varepsilon_1,\varepsilon_2,\varepsilon_3,d_1,d_2,d_3,R_1,R_2,R_3,q_1,q_2,q_3,D_{f1},D_{f2},D_{f3},$$

$$L_1,L_2,L_3,DD)$$

$$=1-\left|\frac{Z_9-\rho_o c_o}{Z_9+\rho_o c_o}\right|^2$$

$$=\alpha_3(f,p_1\%,p_2\%,p_3\%,d_1,d_2,d_3,R_1,R_2,R_3,q_1,q_2,q_3,D_{f1},$$

$$D_{f2},D_{f3},L_1,L_2,L_3,DD) \tag{25}$$

3. Overall Silenced Sound Power Level

The silenced octave sound power level shown in Fig. 1 is

$$SWL_i = SWLO_i - STL_i \tag{26}$$

where the $SWLO_i$ is the original *SWL* at the inlet of an acoustical plenum (or air compressor's pipe outlet), and *i* is the index of the octave band frequency. The STL_i is the muffler's *STL* with respect to the relative octave band frequency. And, the SWL_i is the silenced *SWL* at the outlet of a muffler with respect to the relative octave band frequency. Finally, the overall SWL_T silenced by a muffler at the outlet is

$$SWL_T = 10*\log\{\sum_{i=1}^{6} 10^{SWL_i/10}\}$$

$$= 10*\log\left\{\begin{array}{l} 10^{[SWLO(f=125)-STL(f=125)]/10} + 10^{[SWLO(f=250)-STL(f=250)]/10} \\ +10^{[SWLO(f=500)-STL(f=500)]/10} + 10^{[SWLO(f=1000)-STL(f=1000)]/10} \\ +10^{[SWLO(f=2000)-STL(f=2000)]/10} + 10^{[SWLO(f=4000)-STL(f=4000)]/10} \end{array}\right\} \quad (27)$$

4. Objective Function

By using the formulas of Eqs. (6), (18), (22), (25), and (27), the objective function used in minimizing the broadband noise via the *AIM* technique was established. Moreover, an objective function used in a reliability check of the *AIM* method by maximizing the sound transmission loss of a one-chamber plenum lined with a one-layer sound absorber at a targeted tone of 3000 Hz was also constructed. To achieve a better acoustical performance with lower manufacturing cost, the total weight of sound absorbers was fixed.

1) Maximization of Sound Transmission Loss of a One-chamber Plenum lined with a One-layer Sound Absorber at a Pure Tone (f)

Combining Eq. (6) with Eq. (27), the objective function is

$$OBJ_{111} = STL_1(\bar{X}) \quad (28a)$$

$$\bar{X} = (f,\ p_1\%,\ d_1,\ xx3,\ DD)\ ; \quad (28b)$$

2) SWL_T Minimization for a Broadband Noise

Combining Eq. (6) with Eq. (18) and Eq. (27), the objective function for a one-chamber plenum with a one-layer sound absorber is

$$OBJ_{211} = SWL_T(\bar{\bar{X}}) \quad (29a)$$

$$\bar{\bar{X}} = (p_1\%, d_1, DD) \quad (29b)$$

Combining Eq. (6) with Eq. (22) and Eq. (27), the objective function for a one-chamber plenum with a two-layer sound absorber is

$$OBJ_{212} = SWL_T(\bar{\bar{X}}) \quad (30a)$$

$$\bar{\bar{X}} = (p_1\%, d_1, D_{f1}, DD, xx5, p_2\%, d_2);$$

$$xx5 = L_1/DDL;\ DDL = (DD\text{-}q1\text{-}q2\text{-}DDf) \quad (30b)$$

Combining Eq. (6) with Eq. (25) and Eq. (27), the objective function for a one-chamber plenum with a three-layer sound absorber is

$$OBJ_{213} = SWL_T(\bar{\bar{X}}) \quad (31a)$$

$$\bar{\bar{X}} = (p_1\%, d_1, xx3, DD, xx5, xx6, xx7, p_2\%, d_2, p_3\%, d_3);$$

$$xx3 = D_{f1}/DDL;\ xx5 = L_1/DDL;\ DDL = (DD\text{-}q_1\text{-}q_2\text{-}DDf);$$

$$xx6 = D_{f2}/DDf/(1\text{-}xx3);\ xx7 = L_2/DDL/(1\text{-}xx5) \quad (31b)$$

Similarly, the objective function for a two-chamber plenum with a one-layer sound absorber is

$$OBJ_{221} = SWL_T(\bar{\bar{X}}) \quad (32a)$$

$$\bar{\bar{X}} = (p_1\%, d_1, DD, xxx1, xxx2);$$

$$xxx1 = Lx_1/Lx;\ xxx2 = Ls_1/Ly; \quad (32b)$$

The objective function for a two-chamber plenum with a two-layer sound absorber is

$$OBJ_{222} = SWL_T(\bar{\bar{X}}) \quad (33a)$$

$$\bar{\bar{X}} = (p_1\%,\ d_1,\ D_{f1},\ DD,\ xx5,\ p_2\%,\ d_2,\ xxx1,\ xxx2);$$

$$xx5 = L_1/DDL;\ DDL = (DD\text{-}q_1\text{-}q_2\text{-}DDf);$$

$$xxx1 = Lx_1/Lx;\ xxx2 = Ls_1/Ly; \quad (33b)$$

The objective function for a two-chamber plenum with a three-layer sound absorber is

$$OBJ_{233} = SWL_T(\bar{\bar{X}}) \quad (34a)$$

$$\bar{\bar{X}} = (p_1\%, d_1, xx3, DD, xx5, xx6, xx7, p_2\%, d_2, p_3\%, d_3,$$
$$xxx1, xxx2);$$

$$xx3 = D_{f1}/DDL;\ \text{xx5} = L_1/DDL;\ DDL = (DD\text{-}q_1\text{-}q_2\text{-}DDf);$$

$$xx6 = D_{f2}/DDf/(1\text{-}xx3);\ xx7 = L_2/DDL/(1\text{-}xx5);$$

$$xxx1 = Lx_1/Lx;\ xxx2 = Ls_1/Ly; \quad (34b)$$

Likewise, the objective function for a three-chamber plenum with a one-layer sound absorber is

$$OBJ_{231} = SWL_T(\bar{\bar{X}}) \quad (35a)$$

$$\bar{\bar{X}} = (p_1\%,\ d_1,\ DD,\ xxx1,\ xxx2,\ xxx3,\ xxx4);$$

$$\text{xxx1} = Lx_1/Lx;\ \text{xxx2} = Ls_1/Ly;\ \text{xxx3} = Lx_2/Lx;$$

$$\text{xxx4} = Ls_2/Ly; \quad (35b)$$

Likewise, the objective function for a three-chamber plenum with a two-layer sound absorber is

Table 1. Spectrum of an original sound power level (*SWLO*) inside the outlet tube of the diesel engine.

Frequency - Hz	125	250	500	1000	2000	4000	overall
$SWL = 120 + 10\log_{10}$ kw – (*lex*/1.2) – dB	140.2	140.2	140.2	140.2	140.2	140.2	
Spectrum correction – dB	-3	-7	-15	-19	-25	-35	
A-weighted	-16	-9	-3	-0	+1	+1	
SWLO – dB(A)	121.2	124.2	122.2	121.2	116.2	106.2	121.2

$$OBJ_{232} = SWL_T(\overline{XX}) \tag{36a}$$

$$\overline{XX} = (p_1\%, d_1, D_{f1}, DD, xx5, p_2\%, d_2, xxx1, xxx2, xxx3, xxx4);$$

$$xx5 = L_1/DDL;\ DDL = (DD\text{-}q_1\text{-}q_2\text{-}DDf);\ xxx1 = Lx_1/Lx;$$

$$xxx2 = Ls_1/Ly;\ xxx3 = Lx_2/Lx;\ xxx4 = Ls2/Ly; \tag{36b}$$

Likewise, the objective function for a three-chamber plenum with a three-layer sound absorber is

$$OBJ_{233} = SWL_T(\overline{XX}) \tag{37a}$$

$$\overline{XX} = (p_1\%, d_1, xx3, DD, xx5, xx6, xx7, p_2\%, d_2, p_3\%, d_3, xxx1, xxx2, xxx3, xxx4);$$

$$xx3 = D_{f1}/DDL;\ xx5 = L_1/DDL;\ DDL = (DD\text{-}q_1\text{-}q_2\text{-}DDf);$$

$$xx6 = D_{f2}/DDf/(1\text{-}xx3);\ xx7 = L_2/DDL/(1\text{-}xx5);$$

$$xxx1 = Lx_1/Lx;\ xxx2 = Ls_1/Ly;\ xxx3 = Lx_2/Lx;$$

$$xxx4 = Ls_2/Ly; \tag{37b}$$

III. CASE STUDIES

As indicated in Fig. 1, to depress a noise from a diesel engine, three kinds of multi-chamber acoustical plenums (one-chamber, two-chamber, and three-chamber) shown in Fig. 2 that are internally lined with four kinds of multi-layer sound absorbers shown in Fig. 3 (one-layer, two-layer, three-layer, and four-layer) are considered. The original sound power level (*SWLO*) at the diesel engine's tube outlet is shown in Table 1 where the overall *SWLO* reaches 121.2 dB(A). A sound absorbing material with a flowing resistant (*R*) of 4000 (rayls/m) was adopted. To obtain the best acoustical performance within a fixed space, numerical assessments linked to an *AIM* optimizer were applied. Before the minimization of a broadband noise was executed, a reliability check of the *AIM* method by maximizing the sound transmission loss of a one-chamber plenum lined with a one-layer sound absorber at a targeted tone (3000 Hz) had been carried out. To achieve the lowest cost in the plenum, the outline dimension of the plenum was 2.0 M in length (L_x), 1.0 M in width (L_y), and 0.8 M in height (L_z). Additionally, the plenum outlet is 0.8M * 0.05 M. Moreover, the total thickness of the perforated plate and the sound absorbing material were fixed at 0.003 M and 0.05 M.

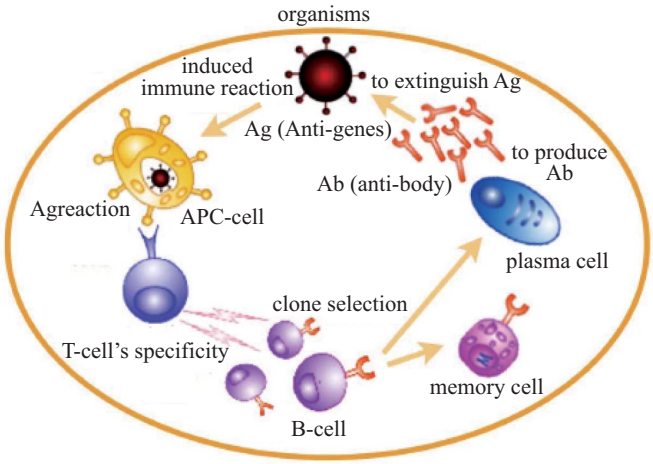

Fig. 4. The immune reaction for a organism.

IV. ARTIFICIAL IMMUNE METHOD

The artificial immune method is originated from the organism's immune system. A book related to the artificial immune method was first published [13]. Also, the papers which were related to the artificial immune method were reorganized [7, 8]. Because the artificial immune method is better in both global and local searching, it has been widely used in various fields to solve optimization problems such as pattern recognition and classification [5], engineering search and optimization methods [12, 23, 26], scheduling [11, 27], data mining [16], and computational security [4, 15].

As indicated in Fig. 4, the antigen appendage cell (*APC*) will perform the antigen appendage reaction when the antigen (*Ag*) invades the organism [18]; thereafter, the killer T lymphocyte (T-cell) will recognize the *Ag* and stimulate the B-cell to select and produce the specific B-cells. When mature, the B-cells will be transformed into a plasma cell and memory cell. Later, the plasma cell will produce antibodies (*Ab*) to extinguish the *Ag*. The plasma cells will be transformed into a suppressor T cell when all the antigens are extinguished. Consequently the immune reaction for the organism is terminated. Here, a specific pathogen may be joined with various anti-bodies. Each anti-body will be connected with one of the anti-gene located on the surface of the pathogen.

The artificial immune method has the characteristics of the adaptive immune reaction, including specificity and adaptability between *Ag* and *Ab*, discrimination of *Ag*, clone

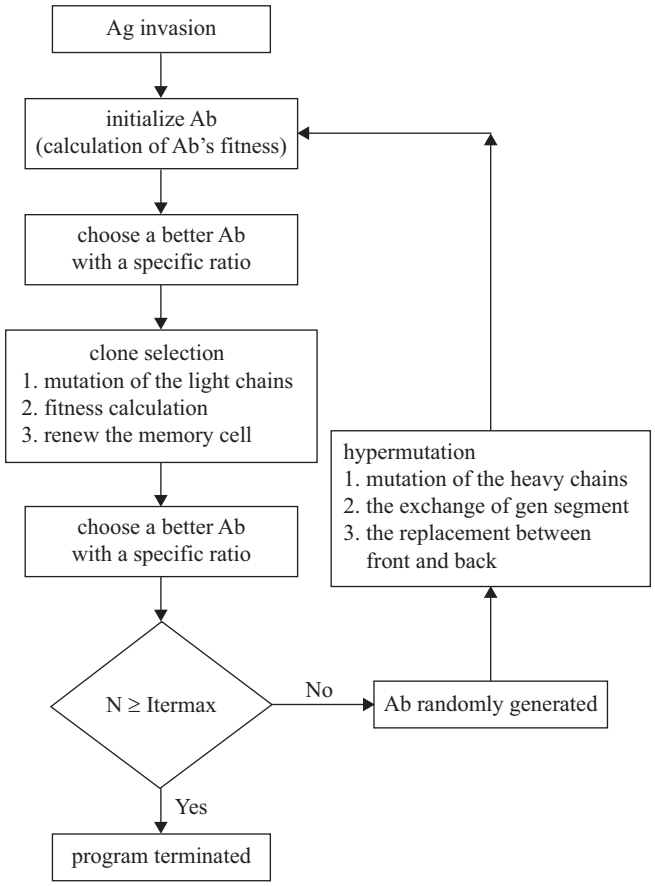

Fig. 5. Flow diagram of the artificial immune method.

selection and memory and cytokine of *Ab*, and somatic recombination/somatic mutation/regeneration of *Ab*'s genes. In the whole immune reaction system, the *Ab* has the recognition specificity of the *Ag*. The lymphatic system will produce the appropriate *Ab* to extinguish the pathogen. When using the immune algorithm in the engineering optimization problem, the problem we solve will be regarded as the *Ag*, and the solution will be *Ab*. Based on the targeted *Ag*, the best *Ag* will be searched for step by step. During the immune optimization, the best gene *Ab* will be selected and put into the memory cell for individual generation. Thereafter, the best genes will be kept and used in the next evolution after the screening process in the memory cell. Each *Ab* coded by binary bits presents one solution. The string length of the *Ab* is composed of design parameters. The flow diagram of the artificial immune method is shown in Fig. 5. In the artificial immune optimization, the operation will be repeated until the integrated iteration reaches a maximal iteration preset in the program.

For the single *OBJ* optimization problem, the mathematical optimization model is

$$Ab = \bar{X} = (x_1, x_2, x_3, ..., x_N) \tag{38}$$

$$Ag = OBJ \tag{39}$$

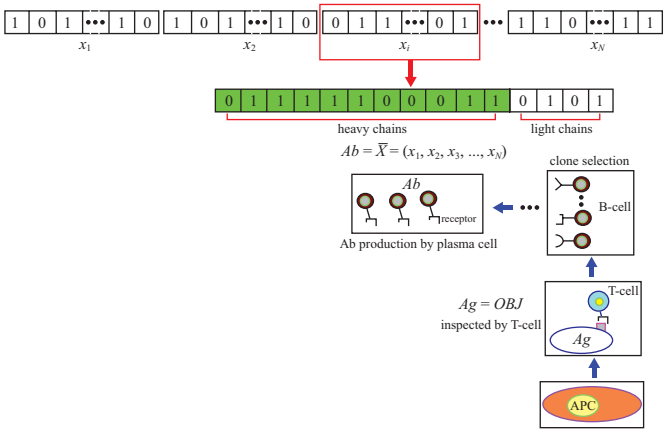

Fig. 6. Relationship between the immune method and the mathematical optimization model.

$$AbAg = OBJ(\bar{X}) \tag{40}$$

where *Ab* is the anti-body, x_N is the *N*-th design parameter, *Ag* is the anti-gene, and *AbAg* is the affinity between the *Ab* and Ag. The relationship mentioned above is shown in Fig. 6.

V. RESULTS AND DISCUSSION

The accuracy of the *AIM* optimization depends on the *abn* (antibody number), the *cn* (clone number), the *maxGen* (max iteration), the *mf* (mutation Factor), the *rmtr* (remove threshold), the *cstr* (clonal selection threshold), and the *div* (diversity). To investigate the influences of the above *AIM*'s control parameters, assessed ranges of the *AIM* parameters are

abn = (10, 30, 50); *cn* = (5, 10, 20); *maxGen* = (10, 20, 30);

mf = (30, 50, 80); *rmtr* = (0.05, 0.1, 0.2);

cstr = (0.005, 0.01, 0.02); *div* =(0.1, 0.3, 0.5).

The results of two optimizations — one, a pure tone noise used for the *AIM*'s accuracy check; and the other, a broadband noise occurring in an air compressor — are described below.

1. Results

1) Pure Tone Noise Optimization

By using Eq. (28), the maximization of the sound transmission loss with respect to a one-chamber plenum lined with a one-layer sound absorber (*R* = 4000 rayls/m) at the specified pure tone (3000 Hz) was performed first. As indicated in Table 2, fifteen sets of *AIM* parameters were tried in the acoustical plenum's optimization. Obviously, the optimal design data can be obtained from the last set of *AIM* parameters at (*abn*, *cn*, *maxGen*, *mf*, *rmtr*, *cstr*, *div*). Table 2 reveals that the optimal design data was obtained at the last set of *AIM* parameters at (50, 20, 30, 50, 0.05, 0.02, 0.1). Using the optimal

Table 2. Optimal results of a one-chamber plenum lined with a one-layer sound absorber with respect to various *AIM* parameters at targeted tones of 3000 Hz.

Item	AIM parameter							Design parameters			STL (dB)
	abn	cn	maxGen	mf	rmtr	cstr	div	p%	d (m)	DD (m)	
1	10	5	20	30	0.2	0.01	0.5	26.5	0.012	0.099	20.9
2	30	5	20	30	0.2	0.01	0.5	37.0	0.008	0.098	22.2
3	50	5	20	30	0.2	0.01	0.5	31.2	0.004	0.092	22.3
4	50	10	20	30	0.2	0.01	0.5	14.9	0.008	0.057	23.3
5	50	20	20	30	0.2	0.01	0.5	7.5	0.015	0.056	23.4
6	50	20	10	30	0.2	0.01	0.5	38.9	0.003	0.097	23.9
7	50	20	30	30	0.2	0.01	0.5	32.8	0.012	0.053	28.7
8	50	20	30	80	0.2	0.01	0.5	15.4	0.013	0.054	28.7
9	50	20	30	50	0.2	0.01	0.5	30.1	0.009	0.054	29.2
10	50	20	30	50	0.1	0.01	0.5	14.5	0.005	0.054	29.2
11	50	20	30	50	0.05	0.01	0.5	12.9	0.014	0.053	29.2
12	50	20	30	50	0.05	0.005	0.5	39.3	0.007	0.054	29.3
13	50	20	30	50	0.05	0.02	0.5	24.2	0.009	0.054	29.3
14	50	20	30	50	0.05	0.02	0.3	28.5	0.013	0.054	29.3
15	50	20	30	50	0.05	0.02	0.1	15.5	0.009	0.054	29.3

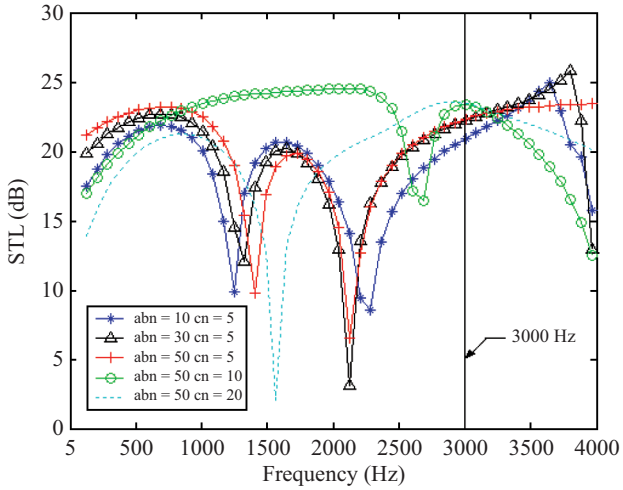

Fig. 7. *STLs* with respect to frequencies at various *AIM* parameters (*abn, cn*) [a one-chamber plenum lined with a one-layer sound absorber] (targeted tone: 3000 Hz).

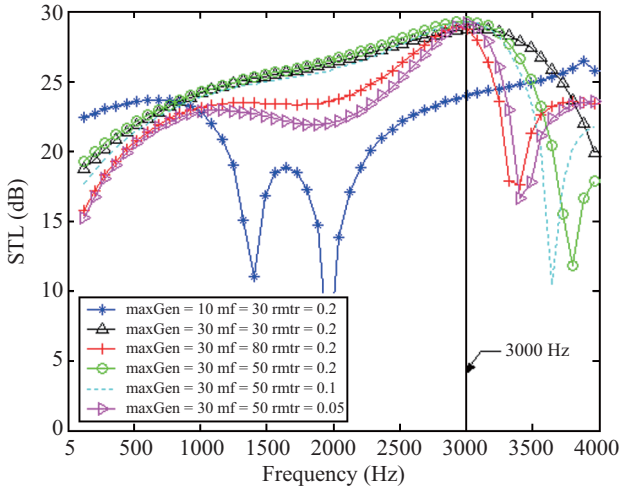

Fig. 8. *STLs* with respect to frequencies at various *AIM* parameters (*maxGen, mf, rmtr*) [a one-chamber plenum lined with a one-layer sound absorber] (targeted tone: 3000 Hz).

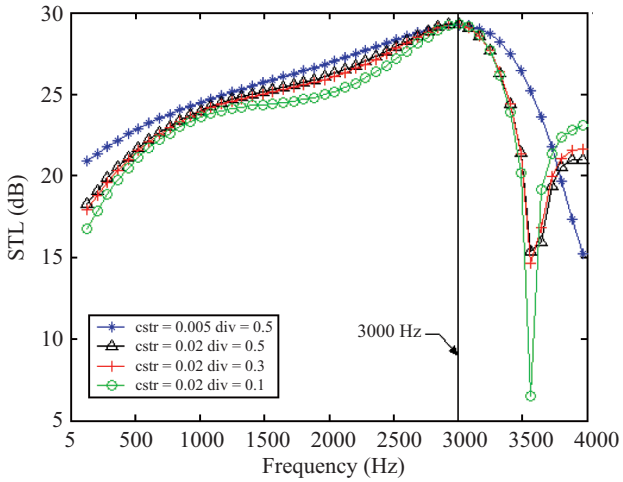

Fig. 9. *STLs* with respect to frequencies at various *AIM* parameters (*cstr, iter*) [a one-chamber plenum lined with a one-layer sound absorber] (targeted tone: 3000 Hz).

design data in a theoretical calculation, the resulting curves of the *STL* with respect to various *AIM* parameters (*abn*, *cn*, *maxGen*, *mf*, *rmtr*, *cstr*, *div*) are depicted in Figs. 7~9. As revealed in Fig. 9, the *STL* is precisely maximized at the desired frequency.

2) Broadband Noise Optimization

To realize the influence of the silenced overall sound power level (SWL_T) with respect to three kinds of multi-chamber plenums (one-chamber, two-chamber, and three-chamber) equipped with three kinds of sound absorbers (one-layer, two-layer, three-layer, four-layer) at the wool's flow resistance (R) of 4000 (rayls/m), formulas of Eqs. (29)-(37) in conjunction with the *AIM* optimizer using the *AIM* parameters of (*abn* = 50, *cn* = 20, *maxGen* = 30, *mf* = 50, *rmtr* = 0.05, *cstr* = 0.02, *div* = 0.1) were performed. The optimal SWL_T of a one-chamber plenum with respect to three kinds of sound absorbers is obtained in Table 3. Similarly, the optimal SWL_T of a two-chamber plenum with respect to three kinds of sound absorbers is obtained in Table 4. Likewise, the optimal resulting SWL_T of a three-chamber plenum with respect to three kinds of sound absorbers is shown in Table 5. Using the optimal design data in a theoretical calculation for three kinds of multi-chamber plenums, the resulting curves of the SWL_T with respect to three kinds of sound absorbers in conjunction

Table 3. Optimal results for a one-chamber plenum equipped with three kinds of multi-layer sound absorbers (broadband noise).

Item	Design parameters						SWL_T – dB(A)
(A) A plenum equipped with a one-layer sound absorber	p%	d(m)	DD(m)				87.9
	39.3	0.0080	0.102				
(B) A plenum equipped with a two-layer sound absorber	p_1%	d_1(m)	D_{f1}(m)	DD(m)	$xx4$	p_2%	79.0
	23.4	0.007	0.010	0.066	0.088	36.2	
	d_2(m)						
	0.005						
(C) A plenum equipped with a three-layer sound absorber	p_1%	d_1(m)	$xx3$	DD(m)	$xx5$	$xx6$	88.2
	31.9	0.014	0.224	0.103	0.960	0.015	
	$xx7$	p_2%	d_2(m)	p_3%	d_3(m)		
	0.153	35.3	0.006	29.9	0.013		

Note: $xx3 = D_{f1}/DDf$; $xx4 = L_1/DDL$; $xx5 = D_{f2}/DDf/(1-D_{f1}/DDf)$; $xx6 = D_{f2}/DDf/(1-D_{f1}/DDf)$; $xx7 = L_2/DDL/(1-L_1/DDL)$
$xx8 = D_{f3}/DDf/(1-D_{f1}/DDf)/(1-xx6)$; $xx9 = L_3/DDL/(1-L_1/DDL)/(1-xx7)$; $DDL = (DD-q1-q2-DDf)$

Table 4. Optimal results for a two-chamber plenum equipped with three kinds of multi-layer sound absorbers (broadband noise).

Item	Design parameters						SWL_T – dB(A)
(A) A plenum equipped with a one-layer sound absorber	p%	d(m)	DD(m)	$xxx1$	$xxx2$		72.0
	39.7	0.006	0.055	0.221	0.876		
(B) A plenum equipped with a two-layer sound absorber	p_1%	d_1(m)	D_{f1}(m)	DD(m)	$xx4$	p_2%	56.3
	29.9	0.009	0.013	0.094	0.261	35.7	
	d_2(m)	$xxx1$	$xxx2$				
	0.008	0.314	0.826				
(C) A plenum equipped with a three-layer sound absorber	p_1%	d_1(m)	$xx3$	DD(m)	$xx5$	$xx6$	64.3
	21.8	0.003	0.449	0.083	0.339	0.186	
	$xx7$	p_2%	d_2(m)	p_3%	d_3(m)	$xxx1$	
	0.344	29.3	0.003	25.2	0.008	0.261	
	$xxx2$						
	0.828						

Note: $xx3 = D_{f1}/DDf$; $xx4 = L_1/DDL$; $xx5 = D_{f2}/DDf/(1-D_{f1}/DDf)$; $xx6 = D_{f2}/DDf/(1-D_{f1}/DDf)$; $xx7 = L_2/DDL/(1-L_1/DDL)$
$xx8 = D_{f3}/DDf/(1-D_{f1}/DDf)/(1-xx6)$; $xx9 = L_3/DDL/(1-L_1/DDL)/(1-xx7)$; $DDL = (DD-q_1-q_2-DDf)$; $xxx1 = Lx_1/L_x$
$xxx2 = Ls_1/L_y$

with the original *SWL* are plotted in Figs. 10~12. Similarly, for a specified layer of sound absorber, the resulting curves of the SWL_T with respect to three kinds of chambers in conjunction with the original *SWL* are plotted in Figs. 13~15. As illustrated in Table 3, the overall sound power levels of a one-chamber plenum with respect to three kinds of sound absorbers will be improved from 121.2 dB(A) to 87.9 dB(A), 79.0 dB(A), and 88.2 dB(A), respectively. Similarly, as illustrated in Table 4, the overall sound power levels of a two-chamber plenum with respect to three kinds of sound absorbers will be improved from 121.2 dB(A) to 72.0 dB(A), 56.3 dB(A), and 64.3 dB(A), respectively. Equally, as illustrated in Table 5, the overall sound power levels of a three-chamber plenum with respect to three kinds of sound absorbers will be improved from 121.2 dB(A) to 75.1 dB(A), 79.7 dB(A), and 60.1 dB(A), respectively.

2. Discussion

To achieve sufficient optimization, the selection of the appropriate *AIM* parameter set is essential. As indicated in Table 2 and Figs. 7~9, the predicted maximal value of the sound transmission loss *STL* for the best *AIM* set of a one-chamber plenum lined with a one-layer sound absorber is precisely located at the desired frequency of 3000 Hz. Therefore, the use of the *AIM* optimization in finding a better design solution is reliable; moreover, three kinds of multi-chamber plenums (one-chamber, two-chamber, and three-chamber) lined with three kinds of sound absorbers (one-layer, two-layer, and three-layer) shown in Fig. 2(A), (B), and (C) are adopted to eliminate the broadband noise.

Table 5. Optimal results for a three-chamber plenum equipped with three kinds of multi-layer sound absorbers (broadband noise).

Item	Design parameters						SWL_T – dB(A)
(A) A plenum equipped with a one-layer sound absorber	p%	d(m)	DD(m)	$xxx1$	$xxx2$	$xxx3$	75.1
	35.5	0.014	0.055	0.520	0.833	0.421	
	$xxx4$						
	0.738						
(B) A plenum equipped with a two-layer sound absorber	p_1%	d_1(m)	D_{f1}(m)	DD(m)	$xx4$	p_2%	79.7
	32.6	0.006	0.027	0.081	0.500	18.2	
	d_2(m)	$xxx1$	$xxx2$	$xxx3$	$xxx4$		
	0.009	0.675	0.762	0.230	0.884		
(C) A plenum equipped with a three-layer sound absorber	p_1%	d_1(m)	$xx3$	DD(m)	$xx5$	$xx6$	60.1
	25.0	0.005	0.031	0.087	0.069	0.155	
	$xx7$	p_2%	d_2(m)	p_3%	d_3(m)	$xxx1$	
	0.626	24.1	0.013	26.2	0.008	0.245	
	$xxx2$	$xxx3$	$xxx4$				
	0.767	0.716	0.828				

Note: xx3 = D_{f1}/DDf; $xx4 = L_1/DDL$; $xx5 = D_{f2}/DDf/(1- D_{f1}/DDf)$; $xx6 = D_{f2}/DDf/(1- D_{f1}/DDf)$; $xx7 = L_2/DDL/(1-L_1/DDL)$
$xx8 = D_{f3}/DDf/(1- D_{f1}/DDf)/(1-xx6)$; $xx9 = L_3/DDL/(1-L_1/DDL)/(1-xx7)$; $DDL = (DD-q_1-q_2-DDf)$; $xxx1 = Lx_1/L_x$
$xxx2 = Ls_1/L_y$; $xxx3 = Lx_2/L_x$; $xxx4 = Ls_2/L_y$

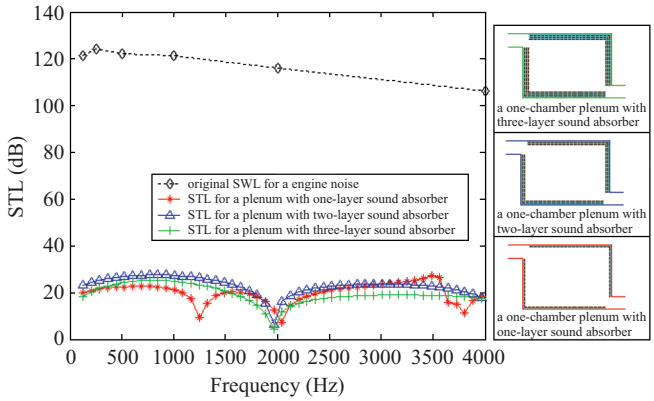

Fig. 10. ***STL*s of one-chamber plenums lined with three kinds of multi-layer sound absorbers (one-layer, two-layer, and three-layer) [wool's flowing resistance = 4000 rayls/m] [broadband noise].**

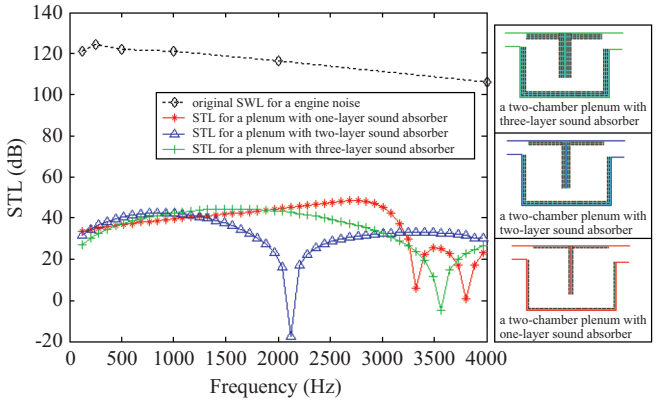

Fig. 11. ***STL*s of two-chamber plenums lined with three kinds of multi-layer sound absorbers (one-layer, two-layer, and three-layer) [wool's flowing resistance = 4000 rayls/m] [broadband noise].**

As indicated in Table 3, the overall sound transmission loss of the optimally shaped one-chamber acoustical plenum with respect to three kinds of sound absorbers reaches 33.3 dB(A), 42.2 dB(A), and 33.0 dB(A). Similarly, as indicated in Table 4, the overall sound transmission loss of the optimally shaped two-chamber acoustical plenum with respect to three kinds of sound absorbers reaches 49.2 dB(A), 64.9 dB(A), and 56.9 dB(A). Equally, as indicated in Table 5, the overall sound transmission loss of the optimally shaped three-chamber acoustical plenum with respect to three kinds of sound absorbers reaches 46.1 dB(A), 41.5 dB(A), and 61.1 dB(A). As indicated in Tables 3~5 and Figs. 10~12, the overall sound transmission loss of the plenum will possibly increase if the number of the layer increases. As can be seen in Figs. 13~15, when using sound absorbers with single layer, the overall

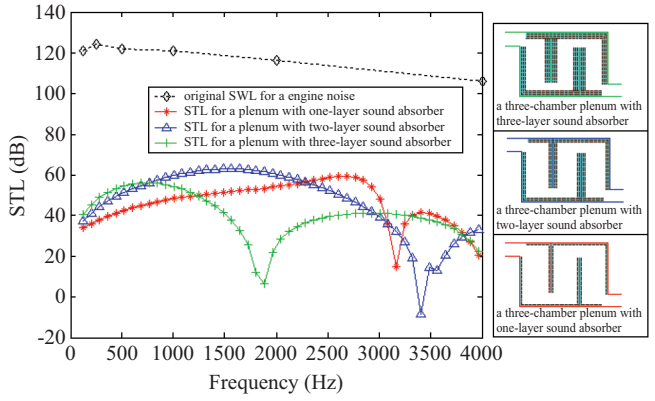

Fig. 12. ***STL*s of three-chamber plenums lined with three kinds of multi-layer sound absorbers (one-layer, two-layer, and three-layer) [wool's flowing resistance = 4000 rayls/m] [broadband noise].**

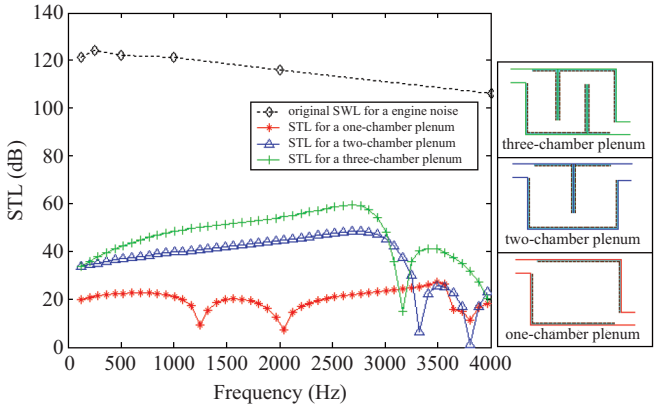

Fig. 13. ***STLs*** **with respect to three kinds of multi-chamber plenums (one-chamber, two-chamber, and three-chamber) lined with a one-layer sound absorber [wool's flowing resistance = 4000 rayls/m] [broadband noise].**

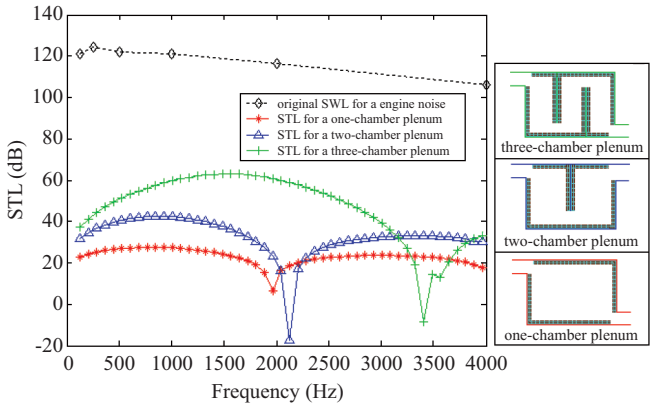

Fig. 14. ***STLs*** **with respect to three kinds of multi-chamber plenums (one-chamber, two-chamber, and three-chamber) lined with a two-layer sound absorber [wool's flowing resistance = 4000 rayls/m] [broadband noise].**

sound transmission loss of the plenum will increase if the number of the plenum's chamber increases.

VI. CONCLUSION

It has been shown that the multi-chamber acoustical plenum lined with multi-layer sound absorber in conjunction with an *AIM* optimizer can be efficiently optimized within a constrained space. As indicated in Table 2, seven kinds of *AIM* parameters (*abn*, *cn*, *maxGen*, *mf*, *rmtr*, *cstr*, and *div*) play essential roles in the solution's accuracy during the *AIM* optimization. As indicated in Fig. 9, the sound transmission loss is precisely maximized at the desired frequency; therefore, the tuning ability established by adjusting the design parameters of the acoustical plenum is reliable. In addition, the appropriate acoustical performance curve of the acoustical plenum in decreasing the overall broadband noise using three chambers (one-chamber, two-chamber, and three-chamber) as well as three sound absorbers (one-layer,

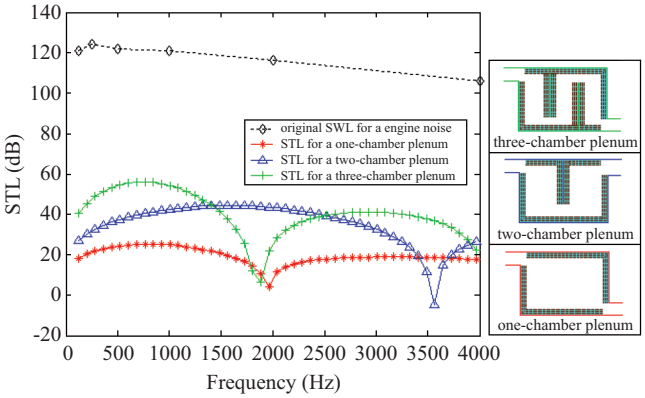

Fig. 15. ***STLs*** **with respect to three kinds of multi-chamber plenums (one-chamber, two-chamber, and three-chamber) lined with a three-layer sound absorber [wool's flowing resistance = 4000 rayls/m] [broadband noise].**

two-layer, and three-layer) has been assessed and shown in Tables 3~5 and Figs. 10~15. As indicated in Figs. 13~15, when using sound absorbers with single layer, the acoustical performance of an acoustical plenum will increase if the number of chamber increases.

Consequently, this approach used for optimally designing the shaped multi-chamber acoustical plenum lined with multi-layer sound absorbers within a constrained space is economical and quite effective.

NOMENCLATURE

This paper is constructed on the basis of the following notations:

Ab	the antibody
Abn	the antibody number
Ag	the antigen
APC	the antigen appendage cell
cn	the clone number
cstr	the clonal selection threshold
C_o	sound speed (m s^{-1})
d_i	diameter of perforated hole on the front plate (m)
dd_k	the diameter from inlet to outlet of the *k*-th chamber plenum
DD	the total thickness of the acoustic panel
D_{fT}	the total thickness of the acoustic fiber
D_{fi}	the thickness of the *i*-layer acoustic fiber
div	the diversity
Ig	the immunoglobulins
j	imaginary unit
k	wave number (= ω/c_o)
k_{1i}	real part of complex $k_{\text{fiber-i}}$
k_{2i}	image part of complex $k_{\text{fiber-i}}$
$k_{\text{fiber-i}}$	complex propagation constant of the *i*-th layer of the acoustic fiber
L_i	air depth of the *i*-th layer of the sound absorber (m)

L_x, L_y, L_z the outline dimension of the plenum (m)
L_{xi} the horizontal distance of the *i*-th baffle within the plenum (m)
L_{si} the vertical depth of the *i*-th baffle within the plenum (m)
maxGen the maximum iteration
mf the mutation factor
N hole's number on the perforated front plate per 1 m^2
OBJ objective function
p_i% porosity of the perforated plate (= ε * 100%) (%)
p_i acoustic pressure at *i* (Pa)
q_i thickness of the i-th layer of the perforated plate (m)
q_T the total thickness of the perforated front plate
R_i acoustic flow resistance of the *i*-th layer of the acoustic fiber (MKS rayls m^{-1})
R_f acoustic flow resistivity of the acoustic fiber (MKS rayls m^{-1})
$R_{fiber\text{-}i}$ real part of the *i*-th layer of complex Z_{fiber}
rmtr the remove threshold
S_e the area of the plenum outlet
STL the sound transmission loss of an acoustical plenum
S_w the total area of the plenum wall
SWL_T the silenced sound power level after adding an acoustical plenum
SWLO the unsilenced sound power level within the compressor outlet
u_i acoustic particle velocity at *i* (kg s^{-1})
$W_{IN\text{-}i}$ the input acoustic power at the inlet of the *i*-chamber plenum (joule s^{-1})
$W_{df\text{-}i}$ the acoustic power in the direct field at the outlet of the *i*-chamber plenum (joule s^{-1})
$W_{OUT\text{-}i}$ the output acoustic power at the outlet of the *i*-chamber plenum (joule s^{-1})
$W_{rf\text{-}i}$ the acoustic power in the reverberant field at the outlet of the *i*-chamber plenum (joule s^{-1})
Z_i specific normal impedance at *i*.
$Z_{fiber\text{-}i}$ characteristic impedance of the *i*-th layer of the acoustic fiber
Z_{pi} characteristic impedance of the *i*-th perforated front plate
$X_{fiber\text{-}i}$ image part of the *i*-th layer of complex $Z_{fiber\text{-}i}$
α_i sound absorption coefficient of the i-layer sound absorber
$\bar{\alpha}_i$ average sound absorption coefficient within a plenum using the *i*-layer sound absorber
ω angular frequency (rad s^{-1})
ϑ_k the angle between the diagonal line for the *k*-th chamber plenum (rad s^{-1})
v kinematic viscosity of air (= $15*10^{-6}$ m^2/s)
ε_i porosity of the *i*-th layer of the perforated plate (m)
δ_i viscous boundary layer thickness of the *i*-th layer of the perforated plate (m)
ρ_o air density (kg m^{-3})
$\rho_o c$ the acoustic impedance

ACKNOWLEDGMENTS

The author acknowledges the financial support of the National Science Council (NSC100-2622-E-235-001-CC3, Taiwan, ROC).

REFERENCES

1. Beranek, L. L. and Ver, I. L., *Noise and Vibration Control Engineering*, John Wiley and Sons, New York (1992).
2. Bie, D. A. and Hansen, C. H., *Engineering Noise Control: Theory and Practice*, Unwin Hyman, London (1988).
3. Blair, G. P. and Coates, S. W., "Noise produced by unsteady exhaust efflux from an internal combustion engine," *SAE*, Report No. 73160 (1973).
4. Brooks, R. A. and Maes, P., "Artificial life IV," *Proceeding of the Fourth International Workshop on the Synthesis and Simulation of Living Systems*, MIT press (1994).
5. Carter, J. H., "The immune system as a model for pattern recognition and classification," *Journal of the American Medical Information Association*, Vol. 7, No. 1, pp. 28-41 (2000).
6. Chang, Y. C., Yeh, L. J., Chiu, M. C., and Lai, G. J., "Shape optimization on constrained single-layer sound absorber by using GA method and mathematical gradient methods," *Journal of Sound and Vibration*, Vol. 286, Nos. 4-5, pp. 941-961 (2005).
7. Dasgupta, D., *Artificial Immune Systems and Their Applications*, Springer-Verlag (1999).
8. de Castro, L. N. and von Zuben, F. J., "Artificial immune systems: part I-basic theory and applications," *Technical Report*, TR-DCA01/99 (1999).
9. Delany, M. E. and Bazley, E. N., "Acoustical properties of fibrous absorbent materials," *Applied Acoustics*, Vol. 13, pp. 105-116 (1969).
10. Ffowcs, J. E. and Howe, M. S., "The generation of sound by density inhomogenities in low mach number nozzle flows," *Journal of Fluid Mechanics*, Vol. 70, No. 3, pp. 605-622 (1975).
11. Fukuda, T., Mori, M., and Tsukiyama, M., "Immune network genetic algorithm for adaptive production scheduling," *Proceeding of the 15th IFAC World Congress*, Vol. 3, pp. 57-60 (1993).
12. Hajela, P., Yoo, J., and Lee, J., "GA based simulation of immune networks-application in structural optimization," *Engineering Optimization*, Vol. 29, pp. 131-149 (1997).
13. Ishida, Y., Hirayama, H., Fujita, H., Ishiguro, A., and Mori, K., *Immunity-based Systems-intelligent System by Artificial Immune Systems*, Corona Pub. Co. Japan (1998). (in Japanese)
14. Jinkyo, L. and Swenson, W. G., "Compact sound absorbers for low frequencies," *Journal Noise Control Engineering Journal*, Vol. 38, pp. 109-117 (1992).
15. Kim, J. and Bentley, P., "Negative selection and niching by an artificial immune system for network instrusion detection," *Proceeding of Genetic and Evolutionary Computation Conference*, pp. 149-158 (1999).
16. Knight, T. and Timmis, J., "AINE: an immunological approach to data mining," *Proceeding of the IEEE International Conference on Data Mining*, pp. 297-304 (2001).
17. Ko, S. H., "Sound attenuation in lined rectangular ducts with flow and its application to the reduction of aircraft engine noise," *Journal of the Acoustical Society of America*, Vol. 50, No. 6, pp. 1418-1432 (1971).
18. Ku, C. C., *Multimodal Topology Optimization of Structure Using Distributed Artificial Immune Algorithm*, Master Thesis, Department of Mechanical Engineering, Tatung University (2003).

19. Lee, F. C. and Chen, W. H., "Acoustic transmission analysis of multi-layer absorbers," *Journal of Sound and Vibration*, Vol. 248, pp. 621-634 (2001).
20. Li, X. and Hansen, C. H., "Comparison of models for predicting the transmission loss of plenum chambers," *Applied Acoustics*, Vol. 66, No. 7, pp. 810-828 (2005).
21. Liu, J. and Herrin, D. W., "Enhancing micro-perforated panel attenuation by partitioning the adjoining cavity," *Applied Acoustics*, Vol. 71, pp. 120-127 (2010).
22. Mccormick, A. M., "The attenuation of sound in lined rectangular ducts containing uniform Flow," *Journal of Sound and Vibration*, Vol. 39, No. 1, pp. 35-41 (1975).
23. Mori, M., Tsukiyama, M., and Fukuda, T., "Immune algorithm with searching diversity and its application to allocation problem," *Transactions of Institute of Electrical Engineering of Japan*, Vol. 113, No. C10, pp. 872-878 (1993).
24. Munjal, M. L., *Acoustics of Ducts and Mufflers with Application to Exhaust and Ventilation System Design*, John Wiley & Sons, New York (1987).
25. Munjal, M. L., "Plane wave analysis of side inlet/outlet chamber mufflers with mean flow," *Applied Acoustics*, Vol. 52, pp. 165-175 (1997).
26. Paton, R., *Computing with Biological Metaphors*, Chapman and Hall (1994).
27. Tomoyuki, M., "An application of immune algorithms for job-shop scheduling problems," *Proceeding of the 5th International Symposium on Assembly and Task Planning*, pp. 146-150 (2003).